Systematics of fusion barriers obtained with a modified proximity potential

Louis C. Vaz*
Departmento de Fisica Nuclear, I.F.U.F.R.J. Cidade Universitaria, Ilha do Fundao, Rio de Janeiro, R. J. Brasil 20.000

John M. Alexander†
Department of Chemistry, State University of New York at Stony Brook, Stony Brook, New York 11794
(Received 30 June 1978)

A systematic semiempirical analysis is presented for excitation functions for complete fusion of complex nuclei. Barrier penetration is included as is the l dependence of the fusion radius. The general form of the proximity potential is assumed and small but important parameter adjustments are made to achieve a fit to experimental data. A correction is presented of s-wave barrier heights and radii for complete fusion. For $Z_tZ_p<500$ these fusion radii are greater than the empirical reaction radii obtained at energies well above the barrier. This result implies weak surface absorption for $Z_tZ_p<500$ and the contrary for higher Z_tZ_p.

[NUCLEAR REACTIONS Semiempirical analysis of complete fusion excitation functions with a modified proximity potential; correlation between s-wave barrier heights and fusion radii; fusion radii exceed empirical interaction radii for $Z_tZ_p<500$ and the contrary.]

I. INTRODUCTION

In the last few years a substantial data base has been accumulated for excitation functions for complete fusion in reactions between complex nuclei (see for example Refs. 1–3). Prior to 1968 there were a variety of means of measuring fission products but the only techniques used for evaporation residues were radiochemical observations of the residual products. Measurements of individual final products were very time consuming, so methods were sought to integrate the cross sections of all the various heavy residual products. In 1968 dielectric track detectors were employed for this purpose,[4] and in 1973 the gas telescope was shown to be extremely useful.[1] More recently the identification of final products by mass has been accomplished by magnetic spectrograph[5] and time of flight measurements.[6] The simultaneous determination of mass and charge has also been achieved for a few cases[7,8] by combinations of these techniques. The great blossoming of these measurements now provides a major probe of the potential between complex nuclei.[2,9-15]

Birkelund and Huizenga have recently collected much of the complete-fusion data and compared them to predictions of the proximity potential without friction.[16] The results show a general consistency with the form of the proximity potential, but a systematic radial shift of 0.1–0.4 fm is indicated. The proximity potential is quite appealing because it provides a simple recipe for the variation of the nuclear potential with the sizes of the collision partners. The three parameters of this global potential have been delimited by the authors' use of much systematic information on nuclear masses, sizes, and skin thicknesses. Therefore the magnitudes of the potential parameters can be expected to be constrained to rather narrow acceptable regions.[15]

In a recent paper[17] we have related the proximity potential to a variety of measurements for the system $^{16}O+^{208}Pb$. We showed that with only small parameter changes one could account for fusion cross sections and the elastic scattering quarter-point angles. In addition, we proposed a sequence of iterative data fitting steps designed to systematically refine the global features of the potential between complex nuclei. In this paper we use the available data for complete fusion to take the first step proposed for this systemization process.

The recent calculations of Birkelund *et al.*[18] based on proximity potential and a one body friction model indicate that at low energies their results differ very little from those obtained by conventional friction free models.[9-12] The latter models assume that at low energies $E \leq E_{lm}^{max}$, fusion occurs after a friction free passage over or through a real potential maximum. We confine our analysis to low energies $E \leq E_{lm}^{max}$, for which the real potential is expected to have a pocket for all reacting waves (as in Ref. 17). For the real nuclear potential we rely on the form of the proximity potential, but alter the value of one of its parameters to fit the excitation functions for complete fusion. The small adjustments of the radius parameter explored here and in Ref. 18 are consistent with the uncertainty of the potential parameters as developed by Blocki *et al.*[15] Nevertheless, these parameter changes imply quite significant alteration of the nuclear potential as discussed for one case in Ref. 17. Finally, we discuss the systematics

of the empirical barrier parameters and their relationship to data and calculations from other sources.[16-19]

II. PROCEDURE FOR ANALYSIS AND COMPARISON TO DATA

A. General framework

The simplest and most commonly used parametrization of fusion cross sections is the classical equation for touching collisions between spheres

$$\sigma_{cf}(E) = \pi R_B^2 (1 - E_B/E) . \quad (1)$$

A plot of $\sigma_{cf}(E)$ vs E^{-1} allows the extraction of two independent parameters R_B and E_B.[1] As discussed in Refs. 17–19, our feeling is that the utilization of the values of R_B so obtained is very hazardous. The reasons are threefold: (a) Equation (1) does not allow for l dependence of the fusion distance.[17,18] (b) Measurements of σ_{cf} may well include increasingly large fractions of interfering products as the energy is lowered.[20] (c) Competing reaction mechanisms may well deplete the fusion process with increasing efficiency as the energy is raised.[11] Therefore we seek another link between the real potential maximum E_{lm} and its radial distance R_m. We obtain this link from the form of the proximity potential and then we only extract one parameter from fitting to fusion cross sections, namely, the fusion barrier E_{0f} for s waves.

The l dependent real potential is written as a sum of Coulomb (C), nuclear (N), and centrifugal parts

$$V(r,l) = V_C(r) + V_N(r) + l(l+1)\hbar^2/2\mu r^2 , \quad (2)$$

where

$$V_C(r) = Z_t Z_p e^2/r , \quad \text{for } r > R_c \quad (3)$$

and

$$V_C(r) = (Z_t Z_p e^2/2R_c)(3 - r^2/R_c^2) , \quad \text{for } r \le R_c \quad (4)$$

with

$$R_c = 1.30\,(A_t^{1/3} + A_p^{1/3}) . \quad (5)$$

The proximity potential for $V_N(r)$ is specified by the parameters R, γ, and b in the following equations[15]:

$$V_N(\zeta) = 4\pi\gamma [C_p C_t/(C_t + C_p)] b \Phi(\zeta) . \quad (6)$$

The dimensionless distance ζ is given by

$$\zeta = (r - C_t - C_p)/b \quad (7)$$

and

$$C = R(1 - b^2/R^2 + \cdots) . \quad (8)$$

The universal potential function $\Phi(\zeta)$ is approximated by

$$\Phi(\zeta) = -0.5(\zeta - 2.54)^2 - 0.0852(\zeta - 2.54)^3 , \quad \text{for } \zeta \le 1.2511 \quad (9)$$

or

$$\Phi(\zeta) = -3.437 \exp(-\zeta/0.75), \quad \text{for } \zeta \ge 1.2511 . \quad (10)$$

Recommended values of the controlling parameters are given as follows[15] with our additions of Δb, $\Delta\gamma$, and ΔR:

$$b = 1.0 + \Delta b , \quad \text{(in fm)} \quad (11)$$

$$\gamma = 0.9517\left(1 - 1.7826\left(\frac{N-Z}{A}\right)^2\right) + \Delta\gamma \quad \text{(in MeV/fm}^2\text{)} \quad (12)$$

$$R = 1.28A^{1/3} - 0.76 + 0.8A^{-1/3} + \Delta R , \quad \text{(in fm)} . \quad (13)$$

For any particular set of the parameters Δb, $\Delta\gamma$, and ΔR, the values are specified for the real potential maximum E_{lm} and its radius R_m.

$$E_{lm} = V_N(R_m) + V_C(R_m) + l(l+1)\hbar^2/2_\mu R_m^2 . \quad (14)$$

The l dependent potential can be approximated near its maximum by a parabola of curvature $\hbar\omega_m$.[21] Transmission coefficients $T_l(E)$ for each partial wave can then be written[17,21]

$$T_l(E) = \{1 + \exp[(2\pi/\hbar\omega_m)(E_{lm} - E)]\}^{-1} , \quad (15)$$

$$\hbar\omega_m = \left| \frac{\hbar^2}{\mu} \frac{d^2V(r,l)}{dr^2} \right|^{1/2}_{R_m, l_{cr}} . \quad (16)$$

The complete fusion cross section follows the conventional summation

$$\sigma_{cf}(E) = \pi\lambda^2 \sum_{l=0}^{\infty} (2l+1) T_l(E) . \quad (17)$$

For any given energy the critical ray (denoted by l_{cr}), for which $T_l(E) = \frac{1}{2}$, is given by the conditions

$$E = V(R_m, l_{cr}) \quad (18)$$

and

$$\left.\frac{dV(r,l)}{dr}\right|_{R_m, l_{cr}} = 0 . \quad (19)$$

From these conditions we have

$$l_{cr} = (R_m/\lambda)[1 - V(R_m)/E]^{1/2} . \quad (20)$$

For l greater than l_{cr}^{max} the real potential no longer has a pocket. This condition is established by the relations

$$\left.\frac{dV(r,l)}{dr}\right|_{l_{cr}^{max}, R_m^{min}} = \left.\frac{d^2V(r,l)}{dr^2}\right|_{l_{cr}^{max}, R_m^{min}} = 0 , \quad (21)$$

We denote the corresponding energy and radius by E_{lm}^{max} and $R_m^{min} \equiv r_m^{min}(A_t^{1/3} + A_p^{1/3})$. As a separate physical model or assumption is required for these

higher energies ($E > E_{lm}^{max}$),[10,11,18] we do not consider them here. We treat only the lower energies and assume that fusion occurs if the barrier is traversed. Also we assume that no significant amount of energy is frictionally dissipated prior to barrier traversal. Inclusion of friction is not expected to alter the systematics of fusion barriers obtained in this work.

Our use of Eqs. (15)–(17) is essentially the same as that of Refs. 14 and 17. The major difference is in the empirical adjustment of the potential. In Ref. 14 it is concluded that the proximity potential fails to describe fusion at near-barrier energies. Here and in Ref. 18 it is shown that with small empirical changes in the radius parameter this potential can correlate the fusion data very well.

In Fig. 1 we show as a function of R_m [or energy via Eq. (18)] the values of the nuclear potential at its maximum, its curvature, and critical l. Values of the curvature $\hbar\omega_m$ vary only slowly with l or R_m until l_{cr} approaches its maximum value (or E approaches E_{lm}^{max}). Then, of course, $\hbar\omega_m$ goes to zero and this simple model breaks down.[22] The discontinuities in $\hbar\omega_m$ occur due to the assumed forms for the Coulomb potential [Eqs. (3) and (4)] and the universal function [Eqs. (9) and (10)]. This is not of central importance for the present study.

For any given set of parameters $\Delta\gamma$, Δb, and ΔR the equations above specify the maximum s-wave barrier height E_{0f} and its corresponding radial position R_{0f}. *Thus E_{0f} and R_{0f} are not independent in our approach.* It is convenient to discuss the parameters R_{0f} and E_{0f} in reduced form (r_{0f} and r_{ef}) as follows:

$$r_{0f} = R_{0f}/(A_t^{1/3} + A_p^{1/3}), \tag{22}$$

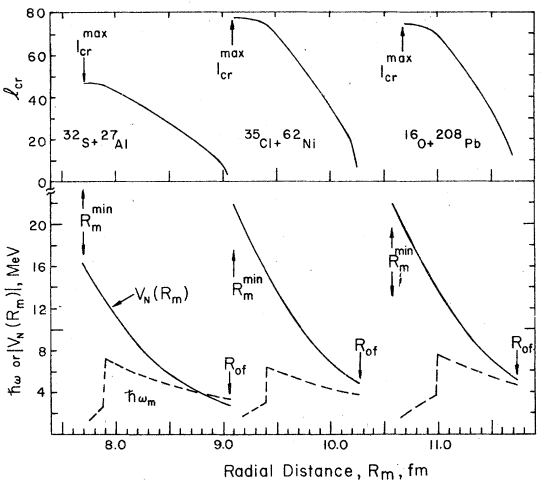

FIG. 1. Variation of l_{crit}, $|V(R_m)|$ and $\hbar\omega_m$ with R_m for the system $^{32}S+^{27}Al$, $^{35}Cl+^{62}Ni$, and $^{16}O+^{208}Pb$. In each case, $\Delta\gamma = \Delta b = 0$ and ΔR from Table II.

$$r_{ef} = Z_t Z_p e^2/E_{0f}(A_t^{1/3} + A_p^{1/3}). \tag{23}$$

It is really these quantities that determine σ_{cf}. The shape of the potential for $r \leq R_m$ and even its curvature $\hbar\omega_m$ play a rather small role.[17]

Our procedure is to specify ΔR, $\Delta\gamma$, and Δb, and then to use Eqs. (2)–(17) to calculate $\sigma_{cf}(E)$. Then we adjust the parameters to achieve a fit, and finally we use Eqs. (14), (22), and (23) to get the s-wave barrier parameters (r_{0f} and r_{ef}), which are most readily systematized.

B. Some aspects of the data fitting

Figures 2 and 3 show some comparisons of calculated to measured fusion cross sections. The dashed lines result from the *a priori* proximity potential with $\Delta\gamma = \Delta R = \Delta b = 0$.[15] In every case, except for the system $^{12}C+^{12}C$, the calculated cross sections are too small or the fusion barriers are too large. Very small changes in the parameters are required to give the reasonable fits shown by the solid curves (Figs. 2, 3). As these parameter changes are very small, we feel that an overall consistency is indicated with the basic trends of

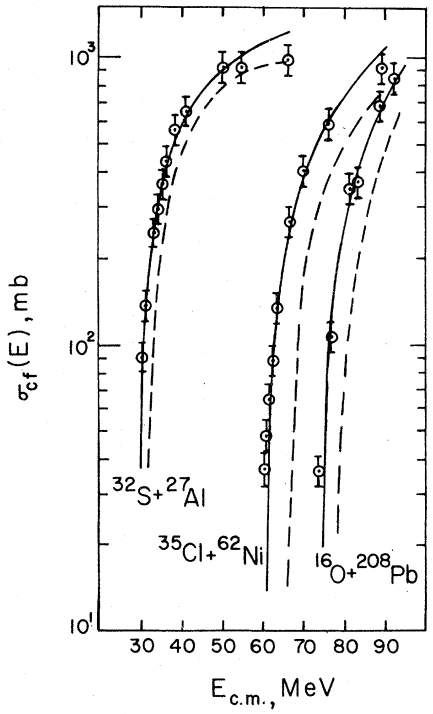

FIG. 2. Comparison of experimental excitation functions for complete fusion with calculation for the systems $^{32}S+^{27}Al$, $^{35}Cl+^{62}Ni$, and $^{16}O+^{208}Pb$. Solid lines represent calculations with the modified proximity potential (see Table II), dashed lines represent calculations with the *a priori* proximity potential ($\Delta R = \Delta b = \Delta\gamma = 0$). Data for systems taken from references indicated in Table II.

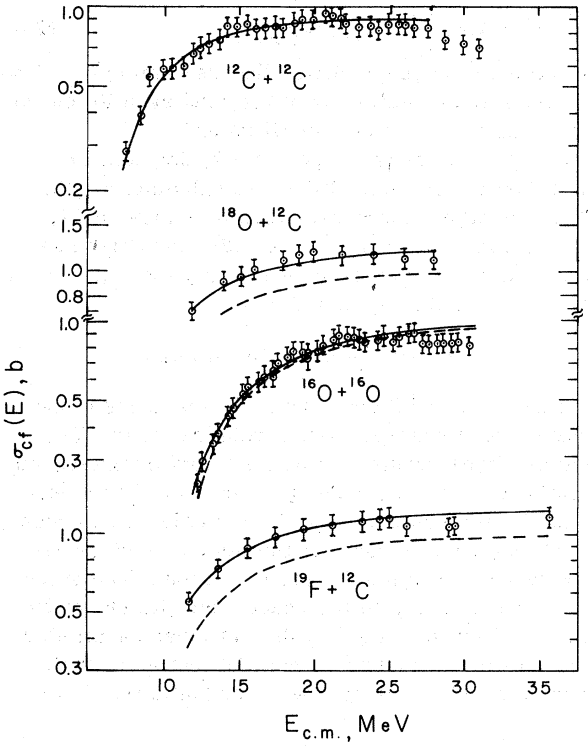

FIG. 3. Comparison of experiment with the calculation for systems $^{12}C+^{12}C$, $^{18}O+^{12}C$, $^{16}O+^{16}O$, and $^{19}F+^{12}C$. See caption of Fig. 2.

III. RESULTS AND DISCUSSION

We have analyzed 48 excitation functions for the potential model.[15,16,18]

What are the sensitivities to each parameter Δb, $\Delta\gamma$, and ΔR? In Figs. 4(a)–4(c) we show calculated excitation functions for $^{16}O+^{208}Pb$ for several choices of each parameter. In each case the calculated curves are shifted in energy but remain roughly parallel. Therefore, we cannot expect to unravel separate roles for γ, b, and R. However,

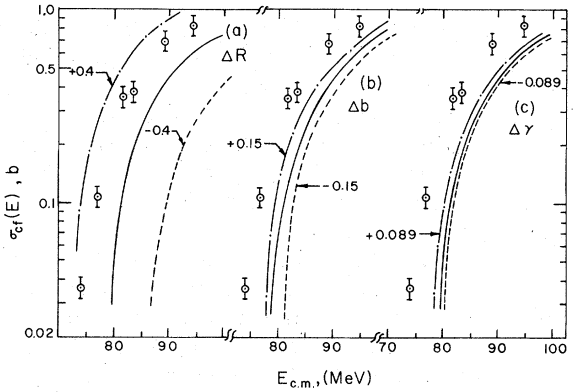

FIG. 4. Calculation of σ_{cf} from Eqs. (15)–(17) with various values for the fitting parameters: (a) $\Delta R=+0.4$ fm, $E_{0f}=72.7$ MeV, $R_{0f}=12.2$ fm; $\Delta R=-0.4$ fm, $E_{0f}=86.9$ MeV, $R_{0f}=10.2$ fm. (b) $\Delta b=+0.15$ fm, $E_{0f}=77.9$ MeV, $R_{0f}=11.2$ fm; $\Delta b=-0.15$ fm, $E_{0f}=81.2$ MeV, $R_{0f}=11.0$ fm. (c) $\Delta\gamma=+0.0887$ MeV fm^{-2}, $E_{0f}=78.9$ MeV, $R_{0f}=11.2$ fm; $\Delta\gamma=-0.0887$ MeV fm^{-2}, $E_{0f}=80.0$ MeV, $R_{0f}=11.0$ fm. Other parameters are $\Delta R=0$ fm, $\Delta b=0$ fm, $\Delta\gamma=0$ MeV fm^{-2}, $E_{0f}=79.4$ MeV, and $R_{0f}=11.1$ fm.

it is clear that variations of ≈10% in γ or b have much smaller effects than ΔR changes of even 0.1 fm. In Table I are given calculated cross sections that result from some combined changes of several of the parameters. We see that the values of E_{0f} and R_{0f} are not changed appreciably for any of these parameter sets that give reasonable fits. For simplicity we choose to set $\Delta\gamma=\Delta b=0$ for all calculations and alter ΔR until the best compromise fit is obtained. Further refinements may provide other combinations of Δb, $\Delta\gamma$, and ΔR that may give a better representation of the potential.[17] Nevertheless, we infer that these values of E_{0f} and R_{0f} obtained here will be very close to those from any improved fit.[17]

In many cases there is a tendency for the data to drop below the calculations at high energy and the reverse at low energies. We will discuss this re-

TABLE I. Effect of parameters ΔR, Δb, and $\Delta\gamma$ on σ_{cf} [a].

	Calculated cross sections (mb)					
$^{16}O+^{208}Pb$	$\Delta b=-0.15$ fm	$\Delta b=-0.15$	$\Delta b=-0.15$	$\Delta b=-0.15$	$\Delta b=0$	Experimental
	$\Delta R=0.358$ fm	$\Delta R=0.381$	$\Delta R=0.336$	$\Delta R=0.34$	$\Delta R=0.23$	cross
	$\Delta\gamma=-0.0354$ MeV fm^{-2}	$\Delta\gamma=-0.0374$	$\Delta\gamma=-0.0335$	$\Delta\gamma=0$	$\Delta\gamma=0$	section
	$E_{0f}=75.36$ MeV	$E_{0f}=75.03$	$E_{0f}=75.70$	$E_{0f}=75.46$	$E_{0f}=75.36$	σ_{cf} [b]
E_{lab} (MeV)	$R_{0f}=11.86$ fm	$R_{0f}=11.92$	$R_{0f}=11.81$	$R_{0f}=11.85$	$R_{0f}=11.74$	(mb)
80	11.65	16.63	8.05	10.45	9.52	36 ± 4
83	103.88	122.19	86.49	98.59	100.45	108 ± 10
88	340.83	361.89	319.94	334.59	333.00	350 ± 40
90	429.47	450.90	408.21	423.12	419.39	377 ± 50
96	670.84	693.25	648.58	664.20	654.06	685 ± 70
102	880.61	903.89	857.49	873.70	857.34	844 ± 90
129.6	1569.08	1595.26	1543.05	1561.31	1519.08	•••

[a] Calculations were made with Eqs. (15)–(17) and a modified proximity potential.
[b] Data from Ref. 23.

TABLE II. Comparison of fusion barrier parameters obtained from Eq. (1) and the present results from this analysis.

		Conventional Analysis [Eq. (1)]			The present analysis										
Reaction	$Z_t Z_p$	R_B (fm)	V_B (MeV)	$-V_N(R_B)$ (MeV)	R_{0f} (fm)	E_{0f} (MeV)	$-V_N(R_{0f})$ (MeV)	ζ_0	$\Phi(\zeta_0)$	$\hbar\omega_0$ (MeV)	$r_m^{\min}$ (fm)	$l_{cr}^{\max}$ ($\hbar$)	$E_{lm}^{\max}$ (MeV)	ΔR (fm)	Ref.
$^{12}C + ^{10}B$	30	...	...	...	7.43	5.23	0.59	3.224	−0.0467	2.53	1.229	14.3	26.04	0.06	26
$^{12}C + ^{11}B$	30	...	...	...	7.46	5.21	0.58	3.232	−0.0462	2.46	1.214	14.8	26.30	0.03	26
$^{12}C + ^{12}C$	36	6.65	6.17	1.63	7.32	6.36	0.73	3.072	−0.0572	2.68	1.200	15.2	27.57	0.00	24
$^{14}N + ^{12}C$	42	7.05	6.7	1.89	7.84	6.98	0.74	3.124	−0.0527	2.62	1.266	18.6	32.46	0.13	28,29,30
$^{16}O + ^{12}C$	48	7.55	7.69	1.46	7.88	7.94	0.84	3.059	−0.0582	2.71	1.262	19.8	34.51	0.12	31
$^{16}O + ^{12}C$	48	7.23	7.94	1.62	7.72	8.09	0.87	3.009	−0.0621	2.76	1.239	19.0	33.54	0.07	27
$^{17}O + ^{12}C$	48	7.27	7.68	1.83	7.88	7.94	0.84	3.056	−0.0585	2.68	1.249	20.1	34.54	0.09	27
$^{18}O + ^{12}C$	48	9.30	7.51	1.28	8.28	7.60	0.76	3.167	−0.0504	2.53	1.295	22.4	37.10	0.19	24
$^{18}O + ^{12}C$	48	7.45	7.55	1.73	8.12	7.73	0.79	3.122	−0.0535	2.58	1.272	21.5	36.00	0.14	27
$^{19}F + ^{12}C$	54	7.64	8.08	2.10	8.32	8.51	0.84	3.104	−0.0547	2.64	1.304	23.4	39.10	0.21	24,25
$^{14}N + ^{16}O$	56	...	...	...	8.09	9.05	0.93	3.022	−0.0611	2.74	1.280	22.4	38.15	0.16	28
$^{16}O + ^{16}O$	64	...	...	...	7.75	10.74	1.15	2.837	−0.0783	2.94	1.223	21.9	38.30	0.03	32
$^{12}C + ^{27}Al$	78	...	...	...	8.31	12.30	1.22	2.850	−0.0779	2.99	1.260	26.2	44.70	0.13	33,34
$^{16}O + ^{27}Al$	104	7.95	16.05	2.79	8.53	16.01	1.54	2.732	−0.0900	3.07	1.260	31.8	52.46	0.15	35,36,37
$^{17}O + ^{27}Al$	104	8.50	15.80	1.82	8.69	15.76	1.49	2.772	−0.0853	2.96	1.267	33.6	53.74	0.17	38,4 36
$^{18}O + ^{27}Al$	104	8.34	15.60	2.36	8.80	15.57	1.45	2.801	−0.0821	2.88	1.272	35.2	54.71	0.18	36
$^{16}O + ^{28}Si$	112	...	...	...	9.13	16.22	1.45	2.838	−0.0782	2.98	1.357	37.1	59.20	0.35	37
$^{4}He + ^{162}Dy$	132	9.9	17.1	2.1	10.28	17.15	1.35	2.559	−0.1074	4.69	1.240	24.2	52.46	0.11	39
$^{32}S + ^{24}Mg$	192	8.5	27.8	4.7	8.96	28.28	2.59	2.439	−0.1330	3.42	1.249	44.1	71.98	0.16	1
$^{7}Li + ^{159}Tb$	195	8.6	23.7	9.0	11.00	23.78	1.74	2.627	−0.1035	4.08	1.279	40.9	74.57	0.26	39
$^{32}S + ^{27}Al$	208	8.3	29.2	6.9	9.06	30.33	2.74	2.411	−0.1380	3.41	1.246	47.0	75.67	0.15	1
$^{35}Cl + ^{27}Al$	221	8.4	30.7	7.2	9.12	32.06	2.88	2.381	−0.1437	3.42	1.240	48.9	78.28	0.13	2
$^{16}O + ^{63}Cu$	232	...	...	...	9.24	33.23	2.94	2.326	−0.1546	3.79	1.225	44.9	78.22	0.08	40
$^{32}S + ^{40}Ca$	320	9.0	43.2	8.0	9.70	43.85	3.68	2.273	−0.1660	3.61	1.277	60.8	96.49	0.26	1
$^{12}C + ^{152}Sm$	372	10.9	46.8	2.3	10.73	46.43	3.49	2.201	−0.1828	4.48	1.243	53.9	99.43	0.16	39
$^{35}Cl + ^{48}Ti$	374	8.7	49.2	12.7	9.49	52.28	4.49	2.112	−0.2057	3.73	1.213	63.4	104.01	0.05	2

TABLE II. (*Continued*)

		Conventional Analysis [Eq. (1)]			The present analysis										
Reaction	$Z_t Z_p$	R_B (fm)	V_B (MeV)	$-V_N(R_B)$ (MeV)	R_{0f} (fm)	E_{0f} (MeV)	$-V_N(R_{0f})$ (MeV)	ξ_0	$\Phi(\xi_0)$	$\hbar\omega_0$ (MeV)	$r_m^{\min}$ (fm)	$l_{cr}^{\max}$ ($\hbar$)	$E_{lm}^{\max}$ (MeV)	ΔR (fm)	Ref.
$^{35}Cl + ^{54}Fe$	442	•••	•••	•••	9.50	61.71	5.29	2.001	−0.2382	3.95	1.198	65.4	113.22	0.02	2
$^{35}Cl + ^{56}Fe$	442	9.5	59.5	7.5	9.77	60.16	5.00	2.061	−0.2202	3.82	1.220	69.5	114.63	0.09	2
$^{32}S + ^{58}Ni$	448	•••	•••	•••	9.62	61.87	5.24	2.016	−0.2339	3.99	1.213	65.6	113.96	0.07	1
$^{35}Cl + ^{58}Ni$	476	9.0	61.3	14.9	10.08	62.94	5.06	2.082	−0.2140	3.83	1.246	74.1	120.22	0.20	2
$^{35}Cl + ^{60}Ni$	476	9.2	61.0	13.5	10.20	62.24	4.94	2.107	−0.2072	3.77	1.252	76.4	121.05	0.22	2
$^{35}Cl + ^{62}Ni$	476	9.6	60.8	10.6	10.27	61.88	4.88	2.117	−0.2043	3.72	1.259	77.8	121.50	0.22	2
$^{35}Cl + ^{64}Ni$	476	9.7	60.3	10.4	10.47	60.80	4.69	2.155	−0.1940	3.64	1.267	81.1	122.54	0.27	2
$^{16}O + ^{148}Nd$	480	9.8	57.8	12.8	10.89	59.13	4.40	2.095	−0.2100	4.41	1.241	65.0	116.03	0.17	39
$^{16}O + ^{150}Nd$	480	•••	•••	•••	10.86	59.26	4.40	2.084	−0.2137	4.41	1.235	63.5	115.40	0.15	39
$^{18}O + ^{148}Nd$	480	9.26	58.3	16.4	10.81	59.51	4.44	2.083	−0.2137	4.21	1.217	68.4	116.98	0.08	39
$^{40}Ar + ^{58}Ni$	504	•••	•••	•••	10.14	66.28	5.30	2.055	−0.2217	3.76	1.232	78.7	125.11	0.15	41
$^{16}O + ^{208}Pb$	656	11.4	74.8	8.2	11.74	75.36	5.15	2.003	−0.2379	4.74	1.253	74.6	137.00	0.23	23
$^{35}Cl + ^{90}Zr$	680	9.8	84.0	15.9	10.74	84.9	6.37	1.954	−0.2541	4.02	1.242	89.5	147.46	0.20	2
$^{40}Ar + ^{109}Ag$	846	•••	•••	•••	10.80	105.01	7.84	1.800	−0.3120	4.14	1.201	97.05	167.10	0.03	42
$^{35}Cl + ^{112}Sn$	850	10.7	105.8	9.0	10.76	105.88	7.94	1.790	−0.3160	4.36	1.213	91.2	166.04	0.08	3
$^{35}Cl + ^{116}Sn$	850	9.8	102.3	22.6	10.84	105.14	7.82	1.799	−0.3124	4.32	1.214	92.8	165.98	0.08	2
$^{35}Cl + ^{120}Sn$	850	10.3	104.9	15.0	10.70	106.38	8.02	1.760	−0.3290	4.35	1.194	90.7	165.19	0.00	3
$^{35}Cl + ^{124}Sn$	850	10.1	104.0	17.2	10.83	105.21	7.83	1.776	−0.3218	4.29	1.199	92.7	164.92	0.02	2
$^{40}Ar + ^{121}Sb$	918	•••	•••	•••	11.01	111.89	8.18	1.776	−0.3220	4.18	1.206	101.7	174.94	0.04	43
$^{35}Cl + ^{141}Pr$	1003	10.4	119.6	19.3	11.09	121.45	8.81	1.714	−0.3498	4.50	1.200	97.1	181.83	**0.04**	3
$^{40}Ar + ^{165}Ho$	1206	•••	•••	•••	11.51	141.25	9.66	1.665	−0.3735	4.88	1.195	110.2	203.66	0.00	43
$^{40}Ar + ^{197}Au$	1422	•••	•••	•••	11.73	163.98	10.40	1.609	−0.4025	4.97	1.177	111.9	223.63	−0.07	44

sult further in the next section and in the Appendixes.

fusion by the methods just described; the parameters that result from this analysis are given in Table II.[1-4,23-44] Columns 3 and 4 give the values of R_B and V_B [Eq. (1)] mostly from Ref. 16 or from appropriate references shown in Table II; columns 6 and 7 give the corresponding values from the present analysis. The fusion barriers (V_B and E_{0f}) differ only slightly, but their radii (R_B and R_{0f}) differ more significantly. This difference is due to our reliance on the proximity potential to link E_{0f} to R_{0f}. The use of Eq. (1) in earlier work has allowed these parameters to be decoupled in the empirical analysis. Note also the differences between $V_N(R_B)$ (column 5) and $V_N(R_{0f})$ (column 8) in Table II.

It is certainly desirable to use the fusion data to obtain two nuclear parameters rather than only one. However, it may be that our current understanding of the reaction mechanisms is not sufficient to give confidence in two independent parameters. We list several problems that are not yet well treated. (a) At near-barrier energies, transfer reaction products are known to be formed in high cross section and projected at small angles.[20] For most experiments to date these would probably be included with the evaporation residues. (b) Static or dynamic deformations of target and/or projectile could lead to enhancement of the subbarrier cross sections.[2,45-47] (c) Deeply inelastic collisions are known to compete with fusing collisions with increasing efficiency as the incident energy is raised.[48]

Each of these effects would operate in the direction of reducing the apparent values of R_B that result from fits of Eq. (1) to the data. Our feeling is that the physical content of the proximity potential gives a stronger basis for analysis than the more conventional use of Eq. (1). As we only extract one parameter from the data [ΔR or, equivalently, the pair E_{0f}, R_{0f} as linked by Eqs. (2)–(14)], we are not really testing the shape of potential itself. We are using it as an equal partner in the systemization of s-wave barriers. This systemization constitutes the first step in a sequence suggested in Ref. 17 for refinement of the potential. The next step is to fit the quarter-point angles measured for elastic scattering. For the system $^{16}O + ^{208}Pb$ (see Ref. 17) this has been achieved by an additional small modification of the parameters ΔR, $\Delta\gamma$, and Δb (while holding E_{0f} essentially fixed). In Table I of Ref. 17 it is shown that these small parameter changes imply significant changes in the nuclear potential. These changes could be quite important for the fusion cross sections at high energies as discussed in the context of other models.[9-12,18]

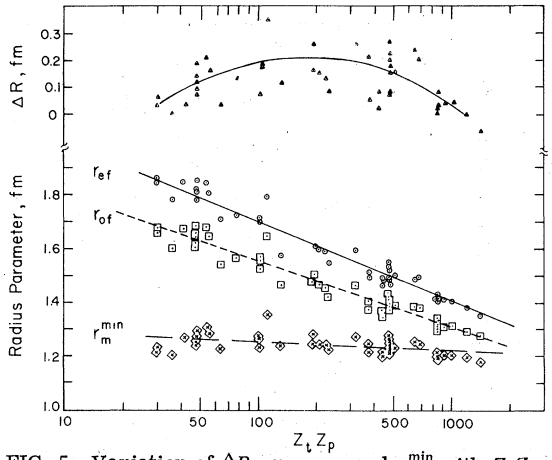

FIG. 5. Variation of ΔR, r_{ef}, r_{0f}, and r_m^{min} with $Z_t Z_p$. Data from Table II.

Now let us examine the trends of the proximity potential as modified by the ΔR values in Table II and in Fig. 5 (upper). We follow the format of Refs. 15, 16, and 18. First, for the system $^{16}O + ^{208}Pb$ we can get a feeling for the radial zone probed by scattering and fusion experiments. In Fig. 6 we plot the values of $V_N(R_m)$ obtained from each fusion datum along with the potential at the rainbow radius, obtained from the scattering data.[17] For each point we have used the same proximity potential; this insures the very smooth trend. Of major interest here is the extent of the range of exploration from 11.4 to 13 fm.

This kind of display can be generalized to all systems[15,16,18] by plotting the modified proximity potential function. We plot in Fig. 7 one point (for each value of E_{0f}, R_{0f}) from each fitted excitation function. As above, the continuity is assured by the use of Eqs. (6) and (7). The point of interest is the range of distances explored (see also Table II, columns 9 and 10).

We turn back to Fig. 5 and the dependence of the s-wave barrier on the reaction system. The fitting parameters ΔR scatter wildly by ≈0.1 fm, but seem to follow a general trend with $Z_p Z_t$. These fluctuations seem to be outside the random errors and may well reflect the individual shell structures and deformations of the collision partners.[2] Figure 5 also shows the various radius parameters plotted against the charge product $Z_p Z_t$. These trends can be described by the following equations:

$$r_{ef} = 2.301 - 0.3003 \log_{10}(Z_t Z_p) \text{ fm}, \quad (24)$$

$$r_{0f} = 2.0337 - 0.2412 \log_{10}(Z_t Z_p) \text{ fm}, \quad (25)$$

$$r_m^{min} = 1.3135 - 0.0315 \log_{10}(Z_t Z_p) \text{ fm}. \quad (26)$$

Recall that r_{ef} comes from the barrier height E_{0f}, r_{0f} is from its radial extent, and r_m^{min} is from the limiting radius for disappearance of the pocket in $V(r, l)$. The decrease of r_{0f} and r_{ef} with $Z_t Z_p$ is

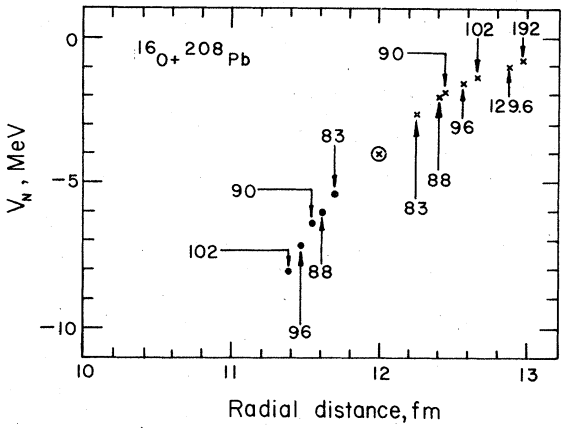

FIG. 6. Variation of the ion-ion potential with distance for the system $^{16}O+^{208}Pb$ (Ref. 17). Bombarding energies are indicated in the figure. Solid circles ● represent the nucleus-nucleus potential deduced from this work, ⊗ from total reactions, and x from elastic scattering (Ref. 17).

expected from the increased Coulomb forces compared to nuclear forces. The approach of r_{0f} to $r_m^{\min}$ for $Z_pZ_t \approx 2000$ implies the disappearance of the s-wave potential pocket. This observation has been often correlated with the failure to observe complete fusion reactions for reaction systems with large values of Z_pZ_t.

Of particular interest is the comparison of these values of r_{0f} to the radius parameters r_0 obtained from reaction cross sections for $E \gg E_{0f}$.[49] (As discussed in Ref. 19 the reaction cross sections generally do not include inelastic scattering.) Recall that the empirical values of r_0 from reaction cross sections do not vary markedly with Z_pZ_t and have a mean value of 1.42 fm.[49] Values of r_{0f} from this study intersect the value of 1.42 fm for $Z_pZ_t \approx 500$. That is to say, for $E \gg E_{0f}$, reactions occur at larger distances than that of the s-wave barrier for $Z_pZ_t \gtrsim 500$ but only inside the s-wave barrier distance for lower Z_pZ_t. This is exactly the same conclusion suggested by comparison to the trends of the elastic scattering data.[17,19] From such a comparison we have concluded that the absorptive potential is strong in the nuclear surface for $Z_pZ_t \gtrsim 1000$ and weak for $Z_pZ_t \lesssim 500$.[17,19]

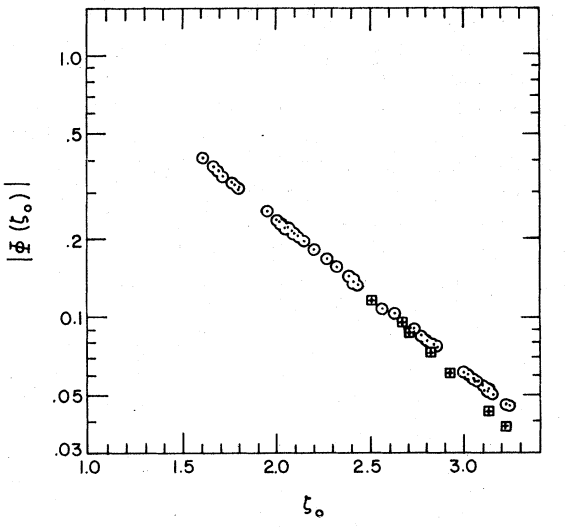

FIG. 7. Points for the reduced potential $|\Phi(\zeta_0)|$ versus (ζ_0) obtained for the systems shown in Table II. Each circle corresponds to an s-wave barrier for one system. Data from scattering for $^{16}O+^{208}Pb$ are given by ⊞.

IV. SUMMARY

We have presented equations for the analysis of fusion cross sections in terms of an assumed real potential. Small modifications of the proximity potential lead to reasonable fits to the data and to a correlation of the barrier parameters with Z_pZ_t. The radial extent (r_{0f}) of the s-wave barrier increases with decreasing charge product. For $Z_pZ_t < 500$ it is greater than the average reaction radius (r_0) for $E \gg E_{0f}$; this implies absorption only in the nuclear interior. For $Z_pZ_t > 500$ this also implies the increasing role of surface absorption.

APPENDIX A: THE POSSIBLE ROLE OF DEFORMATIONS IN THE FUSION CROSS SECTIONS

For most of our fits to fusion excitation functions for $E \lesssim E_{0f}$ we find that Eqs. (15)–(17) underestimate the observed cross section. Often the data could include sizable contributions from transfer reactions after nearly head-on collisions.[20] For measurements from gas telescopes or track detectors the heavy recoils could have been included with the evaporation residues. For $^{16}O+^{208}Pb$ such contamination is not likely as fission provided the signature for fusion.

A more interesting possibility is that the effective Coulomb barrier is lowered by static or dynamic deformations[2,45,46] or by zero-point vibrations.[47] If we assume that either or both of these sources produce a uniform spectrum of barrier heights, then we can estimate the effect of the width (Δ) of this spectrum.[49] We define an average transmission coefficient

$$\langle T_l(E)\rangle = \frac{1}{2\Delta}\int_{E_{0f}-\Delta}^{E_{0f}+\Delta} T_l(E)dE'_{0f}, \tag{27}$$

where $T_l(E)$ is given by Eq. (15). Then the average cross section is given by

$$\langle \sigma_{cf}(E)\rangle = \pi\lambda^2 \sum_{l=0}^{\infty}(2l+1)\langle T_l(E)\rangle. \tag{28}$$

Some examples of the possible effect of such a spectrum of barriers are shown in Fig. 8. For these cases, values of 3.7–4.0 MeV have been used for Δ. Such a wide spectrum of barriers would require very substantial deviations from

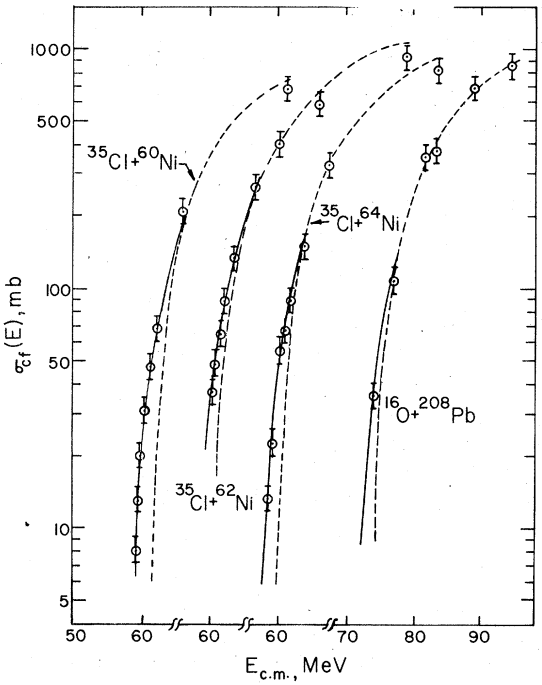

FIG. 8. Comparison of experimental excitation functions for complete fusion with calculation for $E \lesssim E_{0f}$ with $\Delta = 0$ Eq. (17) (dashed line) and Eq. (28) (solid line) for systems $^{35}Cl+^{60}Ni$, $^{35}Cl+^{62}Ni$, $^{35}Cl+^{64}Ni$, and $^{16}O+^{208}Pb$. The values of Δ used in Eq. (28) for these systems are 4.8, 4.0, 3.7, and 3.8 MeV, respectively. Data for these systems were taken from Refs. indicated in Table II.

spherical shapes. If the mean barrier height E_{0f} is reduced slightly then the need for such large Δ values is significantly reduced. Then, however, we would overestimate σ_{cf} above the barrier ($E > E_{0f}$) and would have to invoke competition with other decay channels as competitors with fusion. Sizable changes in the barrier curvatures [$\hbar\omega_m$ in Eq. (16)] could also give the effects shown in Fig. 8. Such changes are outside the spirit of this paper which pursues only small adjustments to the proximity potential.

There are interesting possibilities here, but we feel that their pursuit is best left until the data at these low energies have been reassessed for the possibility of the inclusion of heavy recoils from transfer products.

APPENDIX B: THE RELATIONSHIP BETWEEN VARIOUS FORMULATIONS

For one case $^{16}O+^{208}Pb$ we give a comparison of the calculated fusion cross sections from various formulas (Table III). In each case the parameters are those from Table II (with the inclusion of $\Delta = 3.8$ MeV for column 6). In column 3 the results from Eq. (1) are shown (classical equation with no barrier penetration and fixed radius). Column 4 gives the result of Wong's elaboration of Eq. (1) to include penetrability[50]

$$\sigma_{cf}(E) = (R_{0f}^2/2)(\hbar\omega_0/E) \times \ln\{1+\exp[(2\pi/\hbar\omega_0)(E-E_{0f})]\}. \quad (29)$$

Note that Eq. (29) is identical to the classical result Eq. (1), except at $E \lesssim E_{0f}$. Column 5 gives the result from Eqs. (15)–(17) with the real potential from Eqs. (2)–(14). The addition of penetrability (columns 4 and 5) by either formulation [Eqs. (29) and (17)] gives essentially the same result at near barrier energies. The addition of $\Delta = 3.8$ MeV in Eqs. (27) and (28) raises the near barrier cross sections significantly, column 6. Therefore we agree with Ref. 2 that an extensive set of high-quality data could give interesting information on the effects of deformation on subbarrier fusion cross sections.

TABLE III. Comparison of measured values of σ_{cf} for $^{16}O + ^{208}Pb$ with those calculated by various formulations.

Experiment		Calculation			
E_{lab} (MeV)	σ_{cf}[a] (mb)	σ_{cf}[b] (mb)	σ_{cf}[c] (mb)	σ_{cf}[d] (mb)	σ_{cf}[e] (mb)
80	36 ± 4	•••	10	10	36
83	108 ± 10	96	100	101	119
88	350 ± 40	337	337	333	337
90	377 ± 50	426	426	419	426
96	685 ± 70	670	670	654	670
102	844 ± 90	885	885	857	885
115	•••	1274	1274	1215	1274
129.6	•••	1619	1619	1519	1519

[a] Measurement from Ref. 23.
[b] Calculated with Eq. (1) for all touching collisions.
[c] Calculated with Eq. (29) from Wong (Ref. 50).
[d] Calculated with Eqs. (15)–(17) which use the proximity potential [Eqs. (6)–(14)] and parameters given in Table II.
[e] Calculated with Eqs. (27) and (28) which use a spectrum of barrier heights centered about that for the potential in (d) above.

*The work of L. C. V., was supported by FINEP and CNPQ, Brasil.
†The work of J. M. A. was partially supported by U. S. Department of Energy.

[1] H. H. Gutbrod, W. G. Winn, and M. Blann, Nucl. Phys. A213, 267 (1973).
[2] W. Scobel, H. H. Gutbrod, M. Blann, and A. Mignerey, Phys. Rev. C 14, 1808 (1976), *ibid.* C 11, 1701 (1975).

[3]P. David, J. Bisplinghoff, M. Blann, T. Mayer-Kuckuk, and A. Mignerey, Nucl. Phys. A287, 179 (1977).
[4]L. Kowalski, J. C. Jodogne, and J. M. Miller, Phys. Rev. 169, 894 (1968).
[5]D. Horn, H. A. Enge, A. Sperduta, and A. Graue, Phys. Rev. 17, 118 (1978).
[6]J. D. Garrett, H. F. Wegner, T. M. Cormier, E. R. Cosman, and A. J. Lazzarini, Phys. Rev. C 12, 481(1975)
[7]F. Pühlhofer, W. F. W. Schneider, F. Gasch, J. Barrette, P. Braun-Munzinger, C. K. Gelbke, and H. E. Wegner Phys. Rev. C 14, 1808 (1976); *ibid.* C 11, 1701 (1975). N. Tsoupas, H. Enge, M. Salomaa, A. Sperduto, and A. Graue, Phys. Rev. C 18, 293 (1978).
[8]F. Plasil, R. L. Ferguson, H. C. Britt, R. H. Stokes, B. H. Erkkila, P. D. Goldstone, M. Blann, and H. H. Gutbrod, Phys. Rev. Lett. 40, 1164 (1978).
[9]J. Wilczynski, Nucl. Phys. A216, 386 (1973).
[10]R. Bass, Phys. Lett. 47B, 139 (1973); Nucl. Phys. A231, 45 (1974); Phys. Rev. Lett. 39, 265 (1977).
[11]D. H. E. Gross and H. Kalinowski, Phys. Lett. 48B, 302 (1974); J. Galin, D. Guerreau, M. Lefort, and X. Tarrago, Phys. Rev. C 9, 1018 (1974); D. Glass and U. Mosel, Phys. Rev. C 10, 2620 (1974); Nucl. Phys. A237, 429 (1975).
[12]E. Seglie and D. Sperber, Phys. Rev. C 12, 1236 (1975).
[13]M. Lefort, J. Phys. C-5, 73 (1976), M. Lefort and G. Ngo, Ann. Phys. (Paris) 3, 5 (1978) and references therein.
[14]K. Siwck-Wilczynska and J. Wilczynski, Phys. Lett. 74B, 313 (1978).
[15]J. Blocki, J. Randrup, W. J. Swiatecki, and C. F. Tsang, Ann. Phys. (N. Y.) 105, 427 (1977).
[16]J. R. Birkelund, J. R. Huizenga, Phys. Rev. C 17, 126 (1978).
[17]L. C. Vaz, J. M. Alexander, and E. H. Auerbach, Phys. Rev. C 18, 820 (1978).
[18]J. R. Birkelund, J. R. Huizenga, J. N. De, and D. Sperber, Phys. Rev. Lett. 40, 1123 (1978); J. R. Birkelund and J. R. Huizenga, Proceedings of the Symposium on Heavy-Ion Elastic Scattering, University of Rochester, 1977 (unpublished), p. 210.
[19]L. C. Vaz and J. M. Alexander, Phys. Rev. C 18, 833 (1978).
[20]See, for example, L. Winsberg and J. M. Alexander, Phys. Rev. 121, 518 (1961); R. Bimbot, D. Gardes, and M. F. Rivet, Nucl. Phys. A189, 193 (1973); P. D. Croft, J. M. Alexander, and K. Street, Phys. Rev. 165, 1380 (1968).
[21]D. L. Hill and J. A. Wheeler, Phys. Rev. 89, 1102 (1953); T. D. Thomas, *ibid.* 116, 703 (1959).
[22]For values of $r \leq R_c$ [$= r_c (A_t^{1/3} + A_p^{1/3})$] the functional form of the Coulomb potential changes and this affects slightly the calculated values of R_m, l_{cr}, $\hbar\omega_m$, and E_{lm}. This change is more evident for the values of $\hbar\omega_m$ (see Fig. 1) which decrease less rapidly when calculated with Eq. (4) than when calculated with Eq. (3). As an example, for the system ^{35}Cl+ ^{62}Ni, the calculated values of $R_m^{\min}$, $l_{cr}^{\max}$, $\hbar\omega_{\min}$, $E_{lm}^{\max}$ are 9.10 fm, 77.8 ($\hbar$), 0.72 MeV and 121.5 MeV, respectively, when $r_c = 1.30$ fm and 9.25 fm, 76.2 ($\hbar$), 0.34 MeV and 118.8 MeV, respectively, when $r_c = 1.20$ fm. The same proximity potential (see Table II) was used for both cases. Thus the use of a larger value of the radius parameter r_c causes the maximum energy $E_{lm}^{\max}$ ($l_{cr}^{\max}$) to increase by about 3 MeV [2($\hbar$)] for ^{35}Cl+ ^{62}Ni. The sudden big drop in $\hbar\omega_m$ occurs when the functional forms of the universal function $\Phi(\xi)$ change at $\xi = 1.2511$ ($r = 1.2511\, b + C_t + C_p$). It turns out coincidentally for the cases in Fig. 1 that the universal function changes forms when $r \approx 1.3$ ($A_t^{1/3} + A_p^{1/3}$) with $b = 1$ fm.
[23]F. Videbaek, R. B. Goldstein, L. Grodzins, S. G. Steadman, T. A. Belote, and J. D. Garrett, Phys. Rev. C 15, 954 (1977).
[24]P. Sperr, T. H. Braid, Y. Eisen, D. G. Kovar, F. W. Prosser, Jr., J. P. Schiffer, S. L. Tabor, and S. Vigdor, Phys. Rev. Lett. 37, 321 (1976).
[25]B. Kohlmeyer, W. Pfeffer, and F. Püllhofer, Nucl. Phys. A292, 288 (1977).
[26]M. D. High and B. Cujec, Nucl. Phys. A278, 149 (1977).
[27]Y. Eyal, M. Beckerman, R. Chechik, Z. Fraenkel, and H. Stocker, Phys. Rev. C 13, 1527 (1976).
[28]Z. E. Switkoswski, R. G. Stokstad, and R. M. Wieland, Nucl. Phys. A279, 502 (1976).
[29]R. G. Stokstad, J. Gomez del Campo, J. A. Biggerstaff, A. H. Snell, and P. H. Stelson, Phys. Rev. Lett. 36, 1529 (1976).
[30]R. G. Stokstad, R. A. Dayras, J. Gomez del Campo, and P. H. Stelson, Phys. Lett. 70B, 289 (1977).
[31]P. Sperr, S. Vigdor, Y. Eisen, W. Henning, D. G. Kovar, T. R. Ophel, and B. Zeidman, Phys. Rev. Lett. 36, 405 (1976).
[32]J. J. Kolata, R. C. Fuller, R. M. Freeman, F. Haas, B. Heusch, and A. Gallmann, Phys. Rev. C 16, 891 (1977).
[33]J. B. Natowitz, E. T. Chulick, and M. N. Namboodiri, Phys. Rev. C 6, 2133 (1972).
[34]R. R. Betts, W. A. Langford, M. H. Mortensen, and R. L. White, in Symposium on Macroscopic Features of Heavy Ion Collisions, Argonne National Laboratory, Illinois, 1976 (unpublished).
[35]B. Back, R. R. Betts, C. Gaarde, J. S. Larsen, E. Michelsen, and Tai Kuang-Hshi, Nucl. Phys. A285, 317 (1977).
[36]Y. Eisen, I. Tserruya, Y. Eyal, Z. Fraenkel, and M. Hillman, Nucl. Phys. A291, 459 (1977).
[37]J. Dauk, K. P. Lieband, and A. M. Kleinfeld, Nucl. Phys. A241, 170 (1975).
[38]R. L. Kozub, N. H. Lu, J. M. Miller, and D. Logan, Phys. Rev. C 11, 1497 (1975).
[39]R. Broda, M. Ishihara, B. Herskind, H. Oeschler, S. Ogaza, and H. Rhyde, Nucl. Phys. A248, 356 (1975).
[40]M. Langevin, J. Barrette, and C. Detraz, Phys. Rev. 14C, 152 (1976).
[41]H. H. Gutbrod, F. Plasil, H. C. Britt, B. H. Erkkila, R. H. Stokes, and M. Blann, in *Proceedings of the Third International Atomic Energy Symposium on the Physics and Chemistry of Fission, Rochester 1973* (International Atomic Energy Agency, Vienna 1974), Vol. II, p. 309.
[42]H. C. Britt, B. H. Erkkila, R. H. Stokes, H. H. Gutbrod, F. Plasil, R. L. Ferguson, and M. Blann, Phys. Rev. C 13, 1483 (1976).
[43]J. Peter, F. Hanappe, C. Ngo, and B. Tamain, Report No. INPO-RC-73-07, Orsay (unpublished). Quoted in *Lecture Notes in Physics*, (Springer, Berlin, 1975), Vol. 33, p. 219.
[44]C. Ngo, J. Peter, B. Tamain, M. Berlanger, and F. Hanappe, Z. Phys. A283, 161 (1977).
[45]J. M. Alexander, L. C. Vaz, and S. Y. Lin, Phys. Rev. Lett. 33, 1487 (1974).
[46]H. Freiesleben and J. R. Huizenga, Nucl. Phys. A224, 503 (1974).
[47]P. Kodama, R. A. M. S. Nazareth, P. Moller, and J. R. Nix, Phys. Rev. C 17, 111 (1978).
[48]W. U. Schröder and J. R. Huizenga, Annu. Rev. Nucl. Sci. 27, 465 (1977) and references therein.
[49]L. C. Vaz and J. M. Alexander Phys. Rev. C 10, 464 (1974
[50]C. Y. Wong, Phys. Rev. Lett. 31, 766 (1973).